Stochastic Pulse Regulation in Bacterial Stress Response

James C. W. Locke *et al.*

Science **334**, 366 (2011);
DOI: 10.1126/science.1208144

Science (print ISSN 0036-8075; online ISSN 1095-9203) is published weekly, except the last week in December, by the American Association for the Advancement of Science, 1200 New York Avenue NW, Washington, DC 20005.

Stochastic Pulse Regulation in Bacterial Stress Response

James C. W. Locke,* Jonathan W. Young,* Michelle Fontes,
María Jesús Hernández Jiménez, Michael B. Elowitz†

Gene regulatory circuits can use dynamic, and even stochastic, strategies to respond to environmental conditions. We examined activation of the general stress response mediated by the alternative sigma factor, σ^B, in individual *Bacillus subtilis* cells. We observed that energy stress activates σ^B in discrete stochastic pulses, with increasing levels of stress leading to higher pulse frequencies. By perturbing and rewiring the endogenous system, we found that this behavior results from three key features of the σ^B circuit: an ultrasensitive phosphorylation switch; stochasticity ("noise"), which activates that switch; and a mixed (positive and negative) transcriptional feedback, which can both amplify a pulse and switch it off. Together, these results show how prokaryotes encode signals using stochastic pulse frequency modulation through a compact regulatory architecture.

Gene circuits exhibit fluctuations ("noise") in the concentrations of key components such as transcriptional regulatory proteins (*1*, *2*). Increasingly, noise appears to play functional roles in some systems (*3*–*5*). For example, noise could enable a subpopulation of cells to enter a transient antibiotic-resistant state, enhancing their survival (*6*). However, it remains unclear how genetic circuits use noise to control cellular behaviors. To address this issue, we analyzed σ^B, the transcriptional regulator of general stress response in *Bacillus subtilis*, at the single-cell level (*7*–*9*). Here, we show how σ^B controls its target genes through sustained pulsing, rather than continuous activation; how noise enables this behavior; and how stress levels modulate the frequency of these pulses (Fig. 1A).

Howard Hughes Medical Institute, Division of Biology and Bioengineering, Broad Center, California Institute of Technology, 1200 East California Boulevard, Pasadena, CA 91125, USA.

*These authors contributed equally to this work.
†To whom correspondence should be addressed. E-mail: melowitz@caltech.edu

In prokaryotes, alternative sigma factors form a part of the RNA polymerase holoenzyme, directing it to regulons that control distinct regulatory programs (*10*). σ^B is found in Gram-positive bacteria and impacts pathogenicity in *Listeria monocytogenes* and *Staphyloccous aureus* (*11*, *12*). In *B. subtilis*, σ^B activates more than 150 target genes in response to diverse stresses (*7*, *13*). σ^B is kept inactive by its anti-sigma factor RsbW and is activated by the anti-anti-sigma factor RsbV, which can be reversibly phosphorylated (see Fig. 1B for regulatory interactions). To analyze σ^B activation dynamics, we constructed reporter strains incorporating a yellow fluorescent reporter (*yfp*) for σ^B activity (Fig. 1B) and used quantitative time-lapse microscopy to follow σ^B activation in individual cells (*14*). To quantify σ^B activity in movies, we computed the P_{sigB} promoter activity, defined as the rate of production of yellow fluorescent protein (YFP) [fig. S1A and supporting online material (SOM)].

We first measured the response of σ^B to mycophenolic acid (MPA), an energy stress transduced by RsbQP (fig. S2) (*15*). Constant MPA led to pulses of σ^B activation in individual cells (Fig. 1, C and D, and movie S1). These pulses were unsynchronized across the population, sporadic in time, and sustained, continuing throughout the movie (about six generations) (fig. S3). Similar behavior was observed with other energy stresses and during growth in liquid culture (figs. S1 and S4). Pulses reflected changes in σ^B activity and not intrinsic variability of the P_{sigB} -YFP promoter (fig. S5). Increasing MPA concentration caused a strong increase in pulse frequency, with weaker increases in mean pulse amplitude and duration (Fig. 1E and fig. S6), showing that σ^B is regulated predominantly by frequency modulation (FM) in response to energy stress (Fig. 1A). Pulse amplitudes exhibited broad and monotonically increasing variability with increasing MPA,

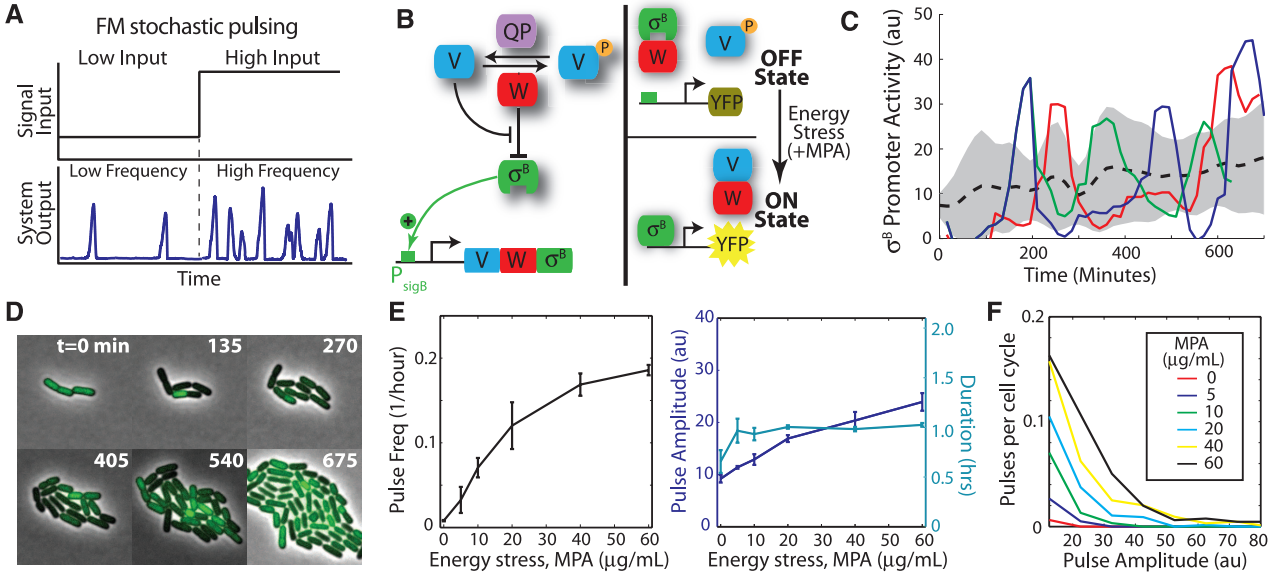

Fig. 1. Energy stress modulates the frequency of stochastic pulses of σ^B activation. (**A**) Schematic of FM pulse regulation. The input signal (black line) controls the frequency of stochastic pulses (blue line, schematic). (**B**) Schematic diagram of σ^B regulatory interactions and states (*7*). When RsbV (V) is phosphorylated (OFF state), σ^B is sequestered by RsbW (W) and inactive (*28*). Under energy stresses such as MPA, RsbV is dephosphorylated by the RsbQP phosphatase complex (QP) (*29*). Other stress inputs are mediated by the RsbTU phosphatase complex (not shown; see SOM text for discussion). Dephosphorylated RsbV can bind to RsbW, releasing σ^B to activate target genes, including its own operon (*30*), and the *yfp* reporter (yellow). (**C**) Promoter activity of the P_{sigB} -YFP reporter pulses in individual lineages (colored solid lines), and its mean and standard deviation across all lineages in four data sets (dashed line and shaded area, respectively). (**D**) Filmstrip of σ^B activation at 60 μg/mL MPA. Heterogeneous expression levels of P_{sigB} -YFP reflect pulsing activity. (**E**) MPA concentration strongly modulates the mean frequency, while more weakly modulating the mean amplitude and duration, of pulses. Error bars, mean ± SEM. (**F**) Pulse amplitude histograms for varying levels of MPA. In (E) and (F), each data point represents data from four microcolonies, acquired on two different days.

with coefficients of variation ranging from 0.16 to 0.70 (Fig. 1F). Together, these results provoke the question of how FM pulse regulation is implemented by the σ^B regulation circuit.

In principle, pulses could be generated in two qualitatively distinct ways: They could arise through amplification of an inherently stochastic underlying process (*16*, *17*). Alternatively, they could result from a limit cycle oscillator whose dynamics become erratic due to noise (*18*). Systematically reducing cellular noise would distinguish between these possibilities, eliminating pulses in the first case but making them more regular in the second case.

To modulate the amplitude of noise in cells, we created strains that could be induced to grow into long multinucleoid filaments by controlling expression of FtsW, a cell division protein necessary for septation. These cells exhibit similar mean expression levels of cellular components (fig. S7) but reduced fluctuations (*19*), allowing us to investigate how reduced noise affects pulse frequency. In time-lapse movies, we observed a systematic decline in pulse frequency in noise-reduced (long) cells across a range of energy stress levels (Fig. 2A and fig. S8), which was also consistent with reduced cell-cell variability in σ^B activity in liquid conditions (Fig. 2B). This reduction in pulse frequency did not reflect reduced sensitivity to MPA, which had a similar effect on growth rate in long and short cells (fig. S8). Together, these results rule out limit cycle models and suggest a noise-dependent mechanism for pulse generation.

How, then, does the σ^B circuit amplify noise to initiate discrete pulses of σ^B activity? To address this question, we analyzed the response of σ^B to increased expression of each circuit component. Up-regulation of kinase (RsbW) and phosphatase (RsbQP) expression had much stronger (opposite) effects on σ^B activity compared with up-regulation of RsbV (fig. S9). This result is interesting because opposing kinase and phosphatase activities can generate sharp, switchlike responses in the phosphorylation of their substrate. An extreme example is zero-order ultrasensitivity, where the phosphatase and kinase operate at saturation (*20*–*22*). We found that σ^B activity exhibited an ultrasensitive response to inducible phosphatase concentration (Fig. 2C and fig. S10), with an effective Hill coefficient of 2.12 [95% confidence interval (CI), n_H = 2.09 to 2.15]. Similar results were also observed with the RsbTU phosphatase (fig. S11). Moreover, this ultrasensitivity was not due to the transcriptional feedback loop. It could be observed in an "open-loop" strain, in which operon expression was inducible and independent of σ^B (fig. S12). In this strain, increasing operon expression led to increasing ultrasensitivity to phosphatase level. These effects could be explained by a minimal mathematical model of the phosphoswitch that does not include the detailed dynamics of the network (see SOM). Finally, consistent with this model, ectopic expression of the kinase RsbW shifted the switching point to higher phosphatase expression levels (fig. S13). This ultrasensitive phosphoswitch could

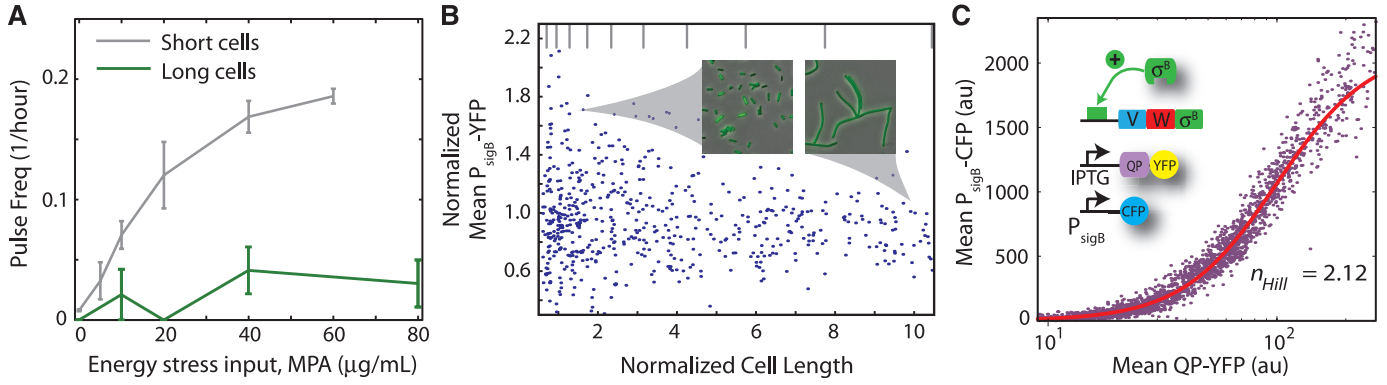

Fig. 2. Pulsing is noise-dependent and involves an ultrasensitive phosphoswitch. (**A**) Pulse frequency in long cells (green) is strongly reduced compared with short cells (gray; data replotted from Fig. 1E). Error bars, mean ± SEM. (**B**) Variability in P_{sigB} -YFP expression decreases with increasing cell length (see fig. S8). Equal numbers of cells (represented by dots) are plotted in each log-spaced bin (delimited by gray vertical lines). (Inset) Overlay of phase contrast and P_{sigB} -YFP expression (green) at different cell lengths. Note greater σ^B variability in short cells. (**C**) σ^B expression is ultrasensitive to RsbQP phosphatase levels. Each dot represents the mean RsbQP-YFP level and P_{sigB} -CFP level of one cell, using the strain shown schematically (table S1). The red line is a Hill function with Hill coefficient n_H = 2.12 (95% CI, n_H = 2.09 to 2.15).

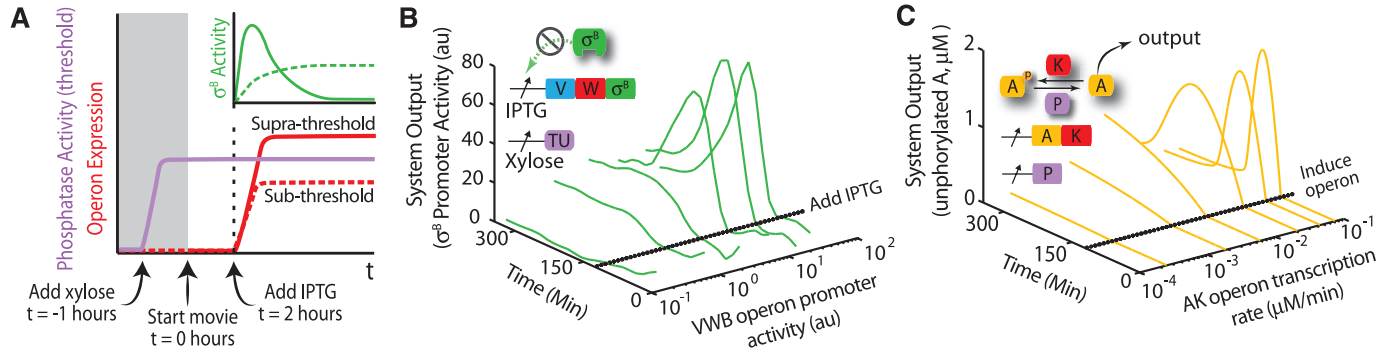

Fig. 3. A mixed transcriptional feedback loop amplifies and terminates pulses. (**A**) Schematic diagram of supra- and subthreshold protocols. Before time-lapse acquisition (gray region), phosphatase is induced to a constant level by addition of xylose. After the start of acquisition, isopropyl-β-D-thiogalactopyranoside (IPTG) is added to induce *rsbVWB* to levels greater than (solid red line) or less than (dashed red line) the level of phosphatase. This results in pulsed (solid green line) or sustained (dashed green line) σ^B activity dynamics. (**B**) σ^B promoter activity exhibits a transition between sub- and suprathreshold behaviors. Each trace shows the mean P_{sigB} promoter activity averaged over four colonies. The promoter activity of the IPTG-inducible σ^B operon (*x* axis) was estimated using a separate strain containing a similar IPTG-inducible *yfp* reporter. Two repeat movies showed similar behaviors. (Inset) Schematic diagram of strain used for this experiment (table S1). (**C**) A minimal mathematical model of the open-loop σ^B network reproduces the main features of the experimental data. (Inset) In this model, the unphosphorylated activator, *A*, directly activates target genes (see SOM).

activate σ^B in response to fluctuations in the phosphatase/kinase ratio and thereby initiate pulses.

How are σ^B pulses further amplified and subsequently terminated? σ^B activates its own operon (*rsbV-rsbW-sigB*). This feedback loop could increase σ^B activity, due to the activating effects of RsbV and σ^B, or it could repress σ^B activity, due to increased production of RsbW. We hypothesized that the phosphoswitch sets a threshold between activating (phosphatase dominant) and repressing (kinase dominant) feedback regimes. As long as phosphatase activity exceeds kinase activity, activation of the operon increases free σ^B (positive feedback). However, this also increases production of RsbW kinase. When kinase activity approaches that of the phosphatase, increased operon expression will cause RsbW levels to cross the threshold, shutting off activation (negative feedback). Thus, autoregulation could result in a "mixed" (positive and negative) feedback loop, providing a compact mechanism to first amplify and then terminate a pulse (*23*).

To test this hypothesis, we constructed an open-loop strain and quantified the change in σ^B activity in response to a step increase in operon expression. In these experiments, we first established a basal level of phosphatase activity in cells and subsequently induced a step, of varying size, in σ^B operon expression (Fig. 3A). We observed a striking transition between two qualitatively different responses: At lower operon induction levels, the system produced a sustained response, whereas at higher induction levels, it exhibited a pulse (Fig. 3B). These results are consistent with the mixed feedback model: Initially, increased operon induction produces more σ^B, which is active due to the high levels of phosphatase, engaging the positive feedback loop. For lower (subthreshold) operon induction levels, RsbW levels never exceed phosphatase levels, so the system remains on indefinitely (Fig. 3A, dashed lines). In contrast, at higher induction levels (superthreshold), RsbW activity eventually crosses the threshold set by the phosphatase and thereby shuts the system off, resulting in a pulse (Fig. 3A, solid lines). Indeed, RsbW dominated other operon components at steady state, suppressing σ^B activity in a dose-dependent manner (fig. S9). In this mechanism, pulse amplitude should be roughly proportional to the difference between the phosphatase level and the kinase level immediately after the initiating fluctuation, as confirmed experimentally (fig. S14). A minimal mathematical model of the circuit exhibited qualitatively similar behavior (Fig. 3C). This mechanism for pulse initiation, amplification, and termination is summarized in Fig. 4, A and B.

These results provoke a final question: How can the cell modulate the frequency of pulses in this system? Systematic changes in the activity of either kinase or phosphatase could modulate the likelihood of threshold-crossing events and thereby control pulse frequency. We first examined the distribution of RsbQP expression levels, using a P_{rsbQP}-rsbQP-YFP protein fusion that complements an RsbQP null mutant (fig. S15). In response to 40 μg/ml MPA, we observed a ~3-fold increase in mean RsbQP-YFP levels, and a ~6-fold increase in mean σ^B activity (fig. S16, A and B). At the single-cell level, RsbQP-YFP expression mapped to σ^B activity (fig. S16C), closely following the (independently determined) ultrasensitive response function (Fig. 2C). These results suggest that stress increases σ^B pulse frequency by increasing the distribution of RsbQP expression levels and thereby increasing the frequency with which RsbQP fluctuations cross the threshold set by RsbW (Fig. 4C). These results do not rule out the complementary possibility, suggested previously (*24*), that some energy stresses may activate σ^B by reducing kinase activity.

To show that this mechanism is indeed sufficient to enable frequency modulation, we rewired the endogenous circuit, replacing RsbQP with an inducible, constitutively active RsbTU phosphatase complex that was unaffected by energy stress (Fig. 4D, inset). The rewired system exhibited stochastic pulsing in response to RsbTU expression (figs. S17 and S18 and movie S2). Furthermore, we observed an increased frequency of pulsing in response to increased RsbTU phosphatase expression (Fig. 4D), with weaker effects on pulse amplitude and duration (fig. S20). These results, qualitatively similar to those observed in wild-type cells under energy stress, also match an extended mathematical model that includes the wild-type transcriptional feedback (gray dashed lines in Fig. 4D, figs. S19 and S20) (see SOM). Thus, modulation of phosphatase expression is sufficient to recapitulate FM pulsing, and no special property of the RsbQP phosphatase is required.

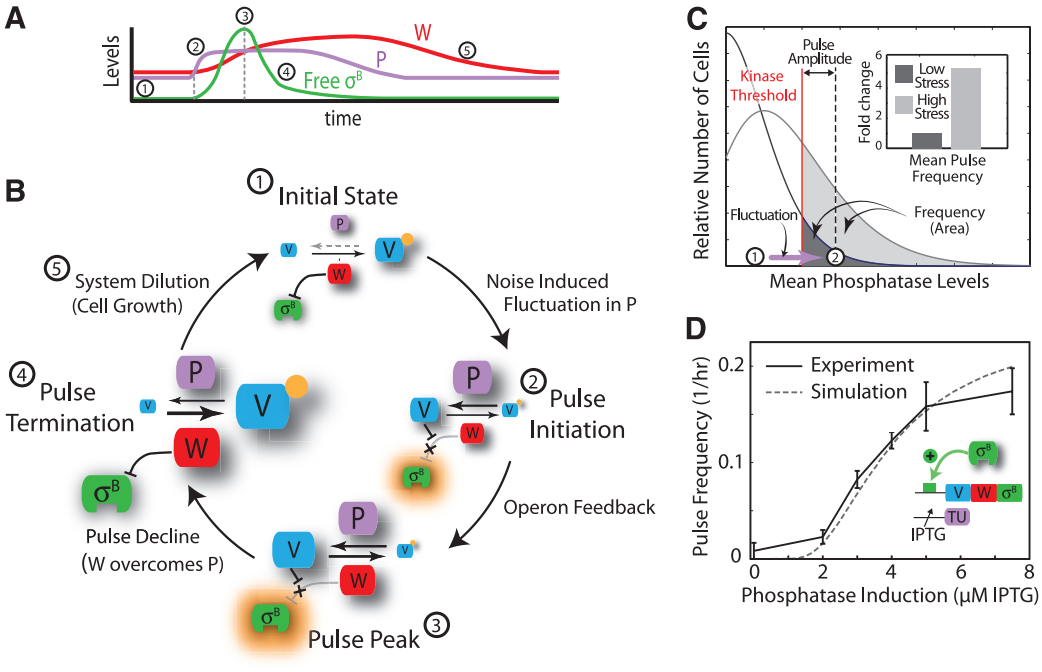

Fig. 4. Mechanism of FM pulse control. (**A**) Schematic time course of phosphatase RsbQP (denoted P, purple), free σ^B (σ^B, green), and kinase (W, red) during a pulse cycle. Circled numbers indicate specific steps in (B). (**B**) Schematic diagram of pulse control. The relative concentration of each component is indicated by size. (1) Initial state: System components are at low levels, kinase activities exceed phosphatase activities, and therefore RsbV is mostly phosphorylated. A threshold-crossing upward fluctuation in RsbQP level dephosphorylates V^P, leading to (2) Pulse Initiation. Activation of σ^B (indicated by glowing halo) leads to up-regulation of operon components (operon feedback). (3) Pulse peak: σ^B activity peaks just before RsbW kinase activity exceeds phosphatase activity. (4) Termination: Rephosphorylation of RsbV shuts the system off. (5) Dilution: Component levels reset to the original state. (**C**) Mechanism of frequency modulation. Fluctuations in phosphatase level (purple arrow from state 1 to 2) can cross the kinase threshold (red line) to initiate a pulse, with amplitude determined by the size of fluctuation (dashed line). Increased stress shifts the distribution of phosphatase levels from lower to higher values (dark and light gray, respectively), increasing the frequency of threshold-crossing events and thereby increasing pulse frequency (inset). (**D**) Tuning of phosphatase expression by IPTG (strain indicated schematically in inset) can regulate pulse frequency. Gray dashed lines show a similar behavior for the mathematical model (fit to data). Each data point represents statistics from two colonies. Two repeat data sets showed similar trends.

FM pulsing can be implemented by a simple circuit of three genes (*rsbW*, *rsbV*, and *sigB*), with input from a phosphatase complex. This system provides a fundamental signal-processing capability to bacterial cells, enabling them to convert steady "DC" inputs into pulsatile, predominantly "AC" outputs. Noise plays a key functional role in this signal processing system (*3*). The σ^B circuit conserves its core architecture in diverse bacteria (*7*), and other alternative sigma factors similarly feature both posttranslational regulation by anti-sigma factors and autoregulatory feedback. Thus, related stochastic pulse modulation schemes are likely employed more generally in bacteria (*10*). The relatively slow time scale of σ^B pulses (Fig. 1E) could confer advantages in responding to unpredictable environments and maintaining a broad, but dynamic, distribution of states in the population through bet-hedging (*25*, *26*). Given the negative effect of σ^B activation on growth rate in some conditions, even under energy stress (*27*), these results suggest that cells balance the benefits and costs of σ^B activation dynamically. It will be interesting to see whether other dynamic encoding schemes are similarly implemented by relatively simple circuit modules.

References and Notes

1. A. Raj, A. van Oudenaarden, *Cell* **135**, 216 (2008).
2. N. Rosenfeld, J. W. Young, U. Alon, P. S. Swain, M. B. Elowitz, *Science* **307**, 1962 (2005).
3. A. Eldar, M. B. Elowitz, *Nature* **467**, 167 (2010).
4. R. Losick, C. Desplan, *Science* **320**, 65 (2008).
5. L. Cai, C. K. Dalal, M. B. Elowitz, *Nature* **455**, 485 (2008).
6. E. Rotem *et al.*, *Proc. Natl. Acad. Sci. U.S.A.* **107**, 12541 (2010).
7. M. Hecker, J. Pané-Farré, U. Völker, *Annu. Rev. Microbiol.* **61**, 215 (2007).
8. W. G. Haldenwang, R. Losick, *Nature* **282**, 256 (1979).
9. O. A. Igoshin, M. S. Brody, C. W. Price, M. A. Savageau, *J. Mol. Biol.* **369**, 1333 (2007).
10. T. M. Gruber, C. A. Gross, *Annu. Rev. Microbiol.* **57**, 441 (2003).
11. M. J. Kazmierczak, S. C. Mithoe, K. J. Boor, M. Wiedmann, *J. Bacteriol.* **185**, 5722 (2003).
12. U. Lorenz *et al.*, *Microbes Infect.* **10**, 217 (2008).
13. M. Hecker, U. Völker, *Mol. Microbiol.* **29**, 1129 (1998).
14. J. C. Locke, M. B. Elowitz, *Nat. Rev. Microbiol.* **7**, 383 (2009).
15. S. Zhang, W. G. Haldenwang, *J. Bacteriol.* **187**, 7554 (2005).
16. A. L. Hodgkin, A. F. Huxley, *J. Physiol.* **117**, 500 (1952).
17. G. M. Süel, J. Garcia-Ojalvo, L. M. Liberman, M. B. Elowitz, *Nature* **440**, 545 (2006).
18. M. B. Elowitz, S. Leibler, *Nature* **403**, 335 (2000).
19. G. M. Süel, R. P. Kulkarni, J. Dworkin, J. Garcia-Ojalvo, M. B. Elowitz, *Science* **315**, 1716 (2007).
20. A. Goldbeter, D. E. Koshland Jr., *Proc. Natl. Acad. Sci. U.S.A.* **78**, 6840 (1981).
21. G. J. Melen, S. Levy, N. Barkai, B. Z. Shilo, *Mol. Syst. Biol.* **1**, 2005.0028 (2005).
22. Z. Cheng, F. Liu, X. P. Zhang, W. Wang, *Biophys. J.* **97**, 2867 (2009).
23. J. C. Ray, O. A. Igoshin, *PLOS Comput. Biol.* **6**, e1000676 (2010).
24. S. Alper, L. Duncan, R. Losick, *Cell* **77**, 195 (1994).
25. M. Acar, A. Becskei, A. van Oudenaarden, *Nature* **435**, 228 (2005).
26. E. Kussell, S. Leibler, *Science* **309**, 2075 (2005).
27. T. Schweder, A. Kolyschkow, U. Völker, M. Hecker, *Arch. Microbiol.* **171**, 439 (1999).
28. A. Dufour, W. G. Haldenwang, *J. Bacteriol.* **176**, 1813 (1994).
29. M. S. Brody, K. Vijay, C. W. Price, *J. Bacteriol.* **183**, 6422 (2001).
30. A. A. Wise, C. W. Price, *J. Bacteriol.* **177**, 123 (1995).

Acknowledgments: We thank C. Price and D. Rudner for providing strains. We thank A. Eldar, R. Kishony, C. Price, N. Wingreen, J. Levine, and other members of M.B.E's laboratory for helpful discussions. Work in M.B.E's laboratory was supported by NIH grants R01GM079771 and P50 GM068763, U.S. National Science Foundation CAREER Award 0644463, and the Packard Foundation. J.C.W.L was supported by the International Human Frontier Science Program Organization and the European Molecular Biology Organization.

Supporting Online Material

www.sciencemag.org/cgi/content/full/science.1208144/DC1
Materials and Methods
SOM Text
Figs. S1 to S20
Table S1
References
Movies S1 and S2

10 May 2011; accepted 1 September 2011
Published online 6 October 2011;
10.1126/science.1208144

Transgenerational Epigenetic Instability Is a Source of Novel Methylation Variants

Robert J. Schmitz,[1,2] Matthew D. Schultz,[1,2,3] Mathew G. Lewsey,[1,2] Ronan C. O'Malley,[2] Mark A. Urich,[1,2] Ondrej Libiger,[4] Nicholas J. Schork,[4] Joseph R. Ecker[1,2,5]*

Epigenetic information, which may affect an organism's phenotype, can be stored and stably inherited in the form of cytosine DNA methylation. Changes in DNA methylation can produce meiotically stable epialleles that affect transcription and morphology, but the rates of spontaneous gain or loss of DNA methylation are unknown. We examined spontaneously occurring variation in DNA methylation in *Arabidopsis thaliana* plants propagated by single-seed descent for 30 generations. We identified 114,287 CG single methylation polymorphisms and 2485 CG differentially methylated regions (DMRs), both of which show patterns of divergence compared with the ancestral state. Thus, transgenerational epigenetic variation in DNA methylation may generate new allelic states that alter transcription, providing a mechanism for phenotypic diversity in the absence of genetic mutation.

Cytosine methylation is a DNA base modification with roles in development and disease in animals as well as in silencing transposons and repetitive sequences in plants and fungi (*1*). In plants, CG methylation is commonly found within gene bodies (*2*–*5*), whereas non-CG methylation, CHG and CHH (where H is A, C, or T), is enriched in transposons and repetitive sequences (*1*). The RNA-directed DNA methylation (RdDM) pathway targets both CG and non-CG sites for methylation and is commonly associated with transcriptional silencing (*6*). This pathway can also target and silence protein-coding genes, giving rise to epigenetic alleles or so-called epialleles that can be heritable through mitosis and/or meiosis (*7*, *8*) and can be dependent on the methylation of a single CG dinucleotide (*9*).

Two meiotically heritable epialleles resulting in morphological variation are the *peloric* (*Linaria vulgaris*) and *colorless non-ripening* (*Solanum lycopersicum*) loci (*10*, *11*). Both show spontaneous epigenetic silencing events within their respective populations (*10*, *12*). However, the frequency at which such spontaneous meiotically heritable epialleles naturally arise in populations is unknown. Although epiallelic variation has been identified between genetically diverse populations within *Arabidopsis thaliana* (*13*), it is unclear whether these identified epialleles are due to underlying genetic variation. Epialleles have also been artificially generated after mutagenesis or because of mutations in the cellular components required for the maintenance of DNA methylation (*14*–*16*).

An *A. thaliana* (Columbia-0) population, the MA lines, derived by single-seed descent for 30 generations (*17*) was used to examine the extent of naturally occurring variation in DNA methylation and the frequency at which spontaneous epialleles emerge over time. We used the MethylC-Seq method (*3*) to determine the whole-genome base resolution DNA methylomes for three ancestral

[1]Plant Biology Laboratory, The Salk Institute for Biological Studies, La Jolla, CA 92037, USA. [2]Genomic Analysis Laboratory, The Salk Institute for Biological Studies, La Jolla, CA 92037, USA. [3]Bioinformatics Program, University of California at San Diego, La Jolla, CA 92093, USA. [4]The Scripps Translational Science Institute and the Department of Molecular and Experimental Medicine, The Scripps Research Institute, La Jolla, CA 92037, USA. [5]Howard Hughes Medical Institute, The Salk Institute for Biological Studies, 10010 North Torrey Pines Road, La Jolla, CA 92037, USA.

*To whom the correspondence should be addressed. E-mail: ecker@salk.edu